Journal of Colloid and Interface Science 402 (2013) 58–67

Contents lists available at SciVerse ScienceDirect

Journal of Colloid and Interface Science

www.elsevier.com/locate/jcis

Carboxymethyl cellulose binding to mineral substrates: Characterization by atomic force microscopy–based Force spectroscopy and quartz-crystal microbalance with dissipation monitoring

Erica Pensini [a], Christopher M. Yip [b], Denis O'Carroll [c], Brent E. Sleep [a,*]

[a] Department of Civil Engineering, University of Toronto, Toronto, ON, Canada M5S 1A4
[b] Department of Chemical Engineering and Applied Chemistry, University of Toronto, Toronto, ON, Canada M5S 3E1
[c] Western University, London, ON, Canada N6A 5B9

ARTICLE INFO

Article history:
Received 17 December 2012
Accepted 31 March 2013
Available online 11 April 2013

Keywords:
Carboxymethyl-cellulose
Silicates
Iron oxides
Attachment
Atomic force microscopy–based force spectroscopy
Quartz-crystal microbalance with dissipation monitoring

ABSTRACT

The attachment of the sodium salt of carboxymethyl cellulose (CMC) onto iron oxide and various silicate substrates in aqueous solution as a function of salt concentration and pH was studied by atomic force microscopy–based force spectroscopy (AFM) and quartz-crystal microbalance with dissipation monitoring (QCM-D). Both ionic strength and cation valency were found to influence substrate binding. Notably, QCM-D experiments strongly suggested that the solubility of CMC is directly impacted by the presence of $CaCl_2$. Such data are critical for the design of new molecules for stabilizing mineral floc dispersions and for assessing the mobility of CMC-coated particles in the subsurface. Modeling of AFM data with an extended Ohshima theory showed that van der Waals and steric forces played a major role in the interactions between CMC and mineral substrates, and that hydration forces were also important.

1. Introduction

The sodium salt of carboxymethyl cellulose (CMC) is a polymer derived from cellulose, yet, unlike cellulose, CMC is soluble in water and chemically reactive (Fig. 1). CMC is neutral at low pH values but hydrolyzes at high pH values. Specifically, at high pH, CMC loses its positive Na^+ counter-ion, acquiring a negative charge. The extent of CMC dissociation is both pH and ionic-strength dependent [1]. Like many other carbohydrates such as starch, guar-gum and dextrin, CMC finds application in a diverse number of industries. It is used to retain water and stabilize dispersions and as a thickener in the cosmetic and food industry [2,3]. In the mineral industry, CMC can be used to both inhibit mineral flotation and stabilize mineral suspensions [4–6]. In order to evaluate the usefulness of CMC either as inhibitor or stabilizer it is important to gain a basic understanding of CMC adsorption onto substrates such as alumina [7], pyrite [8], chalcopyrite [9], molybdenite [10], and talc [9,11–14]. CMC has been used to stabilize titanium nano-particles and zerovalent iron nano-particles, both of which are employed for remediation purposes [15–22]. When particles are employed for remediation purposes, it is important to understand how CMC coatings can affect their mobility in the subsurface. To achieve this goal, it is crucial to probe CMC attachment onto minerals present in the soil.

In order to clearly understand how CMC functions as either a stabilizer or inhibitor of mineral dispersions and how CMC coatings can affect particle mobility in the subsurface, it is important to elucidate the nature of association of CMC with the mineral surface and how this association impacts subsequent interactions. The forces between polymers, such as CMC, and mineral surfaces arise as a consequence of a diversity of interactions, including van der Waals, hydration, electrostatic and steric forces, as well as hydrogen bonding and acid–base interactions. Repulsive steric forces in particular, arise due to compression of the polymer chains [23], and would be clearly dependent on the conformation of the polymer at the mineral surface. We therefore believe that repulsion between polymer-modified substrates is facilitated by polymers that adsorb and adopt an extended conformation protruding perpendicularly from the surface, potentially akin to a brush motif. Since polymer conformation is solvent-dependent, in the case of aqueous solutions, water chemistry (pH, ionic strength) would clearly influence steric forces. This is particularly true for charged polymers that extend away from the surface onto which they are grafted or physisorbed to minimize contact with each other [24].

Neutral in acidic environments, CMC is hydrolyzed under basic conditions, acquiring a negative charge. It is therefore expected that, at high pH, CMC adopts an extended conformation due to

* Corresponding author. Fax: +1 416 978 3674.
E-mail address: sleep@ecf.utoronto.ca (B.E. Sleep).

0021-9797/$ - see front matter © 2013 Elsevier Inc. All rights reserved.
http://dx.doi.org/10.1016/j.jcis.2013.03.053

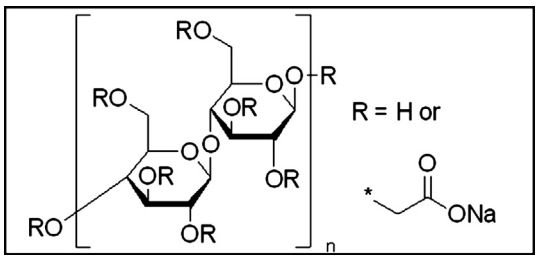

Fig. 1. Structure of the sodium salt of carboxy-methyl cellulose employed in this study.

electrostatic repulsion between the polymer chains. At low pH, CMC is instead more likely to be coiled or collapsed, since the polymer chains are neutral and interchain repulsion decreases. This is consistent with the observation of enhanced swelling of CMC hydrogels under neutral and basic pH conditions [25]. Salts can have an effect similar to low pH values on the polymer conformation due to their ability to participate in electrostatic charge screening [9], which reduces interchain repulsion and favors a coiled conformation [26]. In the case of CMC, both mono- and divalent cations are known to readily associate with the polymer [27–29]. However, divalent salts were found to have a more significant effect than monovalent salts. In particular, it has been reported that the viscosity of CMC solutions decreased significantly in the presence of Ca^{2+} compared with Na^{+} at the same ionic strength [30]. This was attributed to more effective screening by the divalent calcium ion and contraction of CMC chains upon chelation. This effect was reinforced by the observation that the sodium salt of CMC is soluble while its calcium counterpart is insoluble [31]. Based on these data, we believe that aggregation of the CMC occurs in the presence of Ca^{2+}, possibly due to adoption of a coiled conformation for CMC, which promotes flocculation.

Electrostatic forces between polymers such as CMC and mineral surfaces can be affected by the presence of other salts in solution. For example, charge neutralization or reversal in the presence of calcium was hypothesized to promote CMC sorption onto talc [13]. Alternatively, positively charged ions may bind at the negatively charged mineral surfaces, acting as positively charged sites to promote attractive interactions with CMC molecules (bridging effect).

The importance of hydrogen bonding between CMC and mineral surfaces was previously recognized by some authors [3,8], while other researchers propose acid–base interactions as the main sorption mechanism [4]. According to these authors, the characteristics of cations at the mineral surface (valence, radius, and coordination numbers) can affect acid–base interactions by influencing the basic properties of the mineral surfaces. In particular, they report that sorption of certain polymers (such as starch) onto calcium-bearing minerals is particularly favorable. It is noted that both hydrogen bonding and acid–base interactions act at separation distances shorter than electrostatic and van der Waals forces.

To date, the adsorption of CMC onto mineral surfaces has been studied by flotation tests [5,14], atomic force microscopy imaging [3,9], infra-red spectroscopy [3,13], and ToF-SIMS [12,14]. Also, QCM-D studies have been conducted to probe CMC sorption onto cellulose surfaces [32,33], but not onto the materials utilized in the present study. To the best of our knowledge, AFM-based force spectroscopy has only been used to measure the mechanical properties of individual CMC polymers [34]. In the present study, AFM-based force spectroscopy was used to probe the forces of interaction between CMC and several mineral surfaces as a function of water chemistry. The minerals employed in AFM experiments include iron oxide particles and silicate particles (silica, borosilicate, and pumice stone). The silicate particles employed differed in mineral composition and surface roughness, which can affect surface forces. This study allowed assessing if different silicates interact with CMC in a similar manner, or if dissimilarities in surface roughness and mineral composition can have a major impact on the forces of interaction.

Parallel measurements using quartz-crystal microbalance with dissipation monitoring (QCM-D) were performed to assess the reversibility of CMC adsorption onto these surfaces. QCM-D experiments were conducted using magnetite, silica, and aluminum–silicate substrates. Modeling with extended DLVO theory combined with a modified Ohshima's theory [35,36] was conducted to assess the importance of van der Waals and steric forces. Our results will allow theoretical predictions of CMC polymer sorption onto mineral surfaces and may be useful in interpreting experimental studies, for example column adsorption studies, wherein interaction forces cannot be directly measured.

2. Materials and methods

2.1. Atomic force microscopy–based force spectroscopy studies

2.1.1. CMC-coated mica used for AFM studies

CMC polymer coatings were obtained by pipetting 0.1 mL of CMC solution (35 g/L) onto freshly cleaved mica disks. The excess polymer was gently blown off the disks with nitrogen gas, and the polymer solution was allowed to dry. The treatment was repeated at least two times to ensure complete coverage of the mica surface.

2.1.2. Iron oxide particles

Carbonyl iron particles (CIP, Alfa Aesar, product number 10214) were high purity micron-sized iron particles. The CIP were affixed onto AFM cantilevers as described in Section 2.1.4 and aged in pure water (milli-Q water) at room temperature (23 °C) overnight. After aging, the outer core of the particles was a mix of iron oxides and hydroxides, as determined by XPS and EDS analyses. The point of zero charge for aged CIP, ~9, was determined by potentiometric titration in milli-Q water and in 0.1 M $NaNO_3$ salt solution. This value is within the range previously reported for iron oxides [37,38] and nano-iron slurries [39].

2.1.3. Pumice stone particles

Natural pumice stone was crushed using a mortar and pestle to yield particles with a porous surface and irregular structure ranging in diameter from about 1–2.5 μm as determined by scanning electron microscopy (JEOL JSM6610-Lv). The mineral composition of the pumice stone was determined using powder X-ray diffraction (XRD), using a Philips XRD system equipped with a PW 1830 HT generator, a PW 1050 goniometer and PW3710 control electronics. Pumice stone was mainly quartz (SiO_2), with minor amounts of tobermorite (Ca_4Si_6). The particles were negatively charged up to a pH of 2.7, as determined through potentiometric titration conducted in Milli-Q water (titrations were not conducted at lower pH values). This result is consistent with the fact that the

Table 1
Zeta potential of pumice stone particles in different water chemistries.

Solution	pH	Average zeta potential (mV)	Standard deviation (mV)
Milli-Q	5.5	−22.4	5.4
Milli-Q	4	−16.6	5.0
Milli-Q	8	−27.2	5.9
NaCl, 100 mM	5.5	−25.5	0
CaCl2, 100 mM	5.5	−0.5	0

particles were mainly silica, the PZC of which is at acidic pH (~2, cf. 2.2.2). The zeta potential of the particles was also measured in all solutions used in experiments conducted using pumice stone particles (Table 1). The zeta potential was lowest in milli-Q water at pH 8 (-27.2 ± 5.9) and highest in 100 mM $CaCl_2$ solutions (-0.5 ± 0.0), likely due to sorption of Ca^{2+} cations at the pumice surface.

2.1.4. AFM cantilever characteristics and functionalization

Tipless silicon nitride AFM cantilevers were purchased from Bruker (model NP-O10). Their average spring constant (k_c) of ~0.096 nN/nm was determined by the end-massing method [40]. Pumice stone particles and CIP were individually affixed onto these cantilevers using an optical microscope equipped with a micromanipulator. Cantilevers functionalized with silica and 5 μm diameter borosilicate glass particles were purchased from Novascan Technologies Inc. The silica and borosilicate particles were quite smooth, as observed using scanning electron microscopy. The average spring constants of these cantilevers were 0.095 nN/nm and 0.081 nN/nm for the borosilicate and the silica functionalized cantilevers, respectively, determined with the end-massing method.

2.1.5. Aqueous solutions

Water used in this study was treated with a Millipore system (milli-Q water) and had a resistivity of 18.2 mΩ cm. Experiments were conducted in various solutions (pH 5.5, 100 mM NaCl; pH 5.5 100 mM $CaCl_2$; pH 8, milli-Q water buffered with $NaHCO_3$; pH 4, milli-Q water buffered with acetate buffer).

2.1.6. AFM methods and data analysis

All AFM force spectroscopy data were acquired at a scan rate of 1 Hz with a maximum applied load of ~14 nN using a Nanoscope Multimode AFM (Bruker Nano-Surfaces) equipped with a Nanoscope IIIA controller, a glass fluid cell, and a J-scanner running version 5.30a of the Nanoscope software. In a force spectroscopy experiment, from the vertical deflection of the AFM cantilever, it is possible to deduce information about the forces of interaction prior to contact (approach curves) and the adhesive force, i.e., the pull-off force required to detach the particle from the substrate after contact has occurred (retract curves). The conversion from cantilever deflection (δ) to force (F) can be done using Hooke's law [41], given by $F = -k_c \cdot \delta$, where k_c is the spring constant of the cantilever. It is noted that in AFM measurements, there is hysteresis between approach and retract curves and adhesive forces are stronger than approach forces [41]. When the interacting surfaces are polymer coated, different rupture events are recorded as the cantilever is separated from the substrate. Each of these detachment events appears as local minimum in the retract curve, which has a typical saw-tooth shape. The detachment of the last polymer strand from the mineral particle corresponds to the minimum of the curve measured at the separation distance beyond which the retract curve plateaus, indicating complete detachment between the two (Fig. 2a). This minimum was taken as the adhesive force between CMC and mineral particles.

To obtain force vs. distance plots, the raw AFM curves must be registered relative to the point of contact and interpreted to convert the AFM cantilever deflection into a force. When jump to contact occurred, the approach force curves were registered relative to that point. If no local minimum could be located in the approach curve, an imaginary point of contact was defined as the intersection between the lines obtained by fitting the hard-contact portion of the curve and the horizontal line reflecting the off-surface, undeflected tip position (Fig. 2b). The point of contact was denoted as $x = 0$. All approach force data reported in the following discussion refer to the forces measured at the point of contact. All forces were normalized with respect to the particle radius by dividing each point by the particle's radius.

Before each measurement, the cell was rinsed off with the solution of interest to ensure that any CMC loosely attached onto mica was expelled from the cell. In this study, the mineral particles were contacted with CMC polymer coated substrates, and CMC transfer from the substrate to the particles during the measurements cannot be discounted. However, the transfer is expected to be minimal and in any case not sufficient to significantly affect the measurements. It is noted that over 100 approach and retract curves were collected for each water chemistry and the magnitude of the forces measured during subsequent approach–retract cycles was similar. Moreover, we conducted control experiments using bare mica disks. It was verified that significant differences existed between the force curves measured with CMC-coated mica and those measured with bare mica.

2.1.7. Modified Ohshima's model

Ohshima's model describes the interactions between surfaces in terms of van der Waals (F_{VdW}), electrostatic forces ($F_{electro}$), and Born forces (F_{Born}). The expressions for such forces between a sphere and a planar surface are as follows:

$$F_{electro} = 128R\gamma_{sphere}\gamma_{plane}nk_BT\kappa^{-1}\exp(-\kappa d) \tag{1}$$

$$F_{Born} = -\frac{A\sigma^6}{7560}\left[\frac{1}{(2R+7)^7} - \frac{6\cdot(6R-d))}{d^8} - \frac{1}{d^7}\right] \tag{2}$$

$$F_{VdW} = -\frac{AR}{6d^2\left(1+\frac{14d}{\lambda}\right)} + \frac{AR\cdot(14/\lambda)}{6d^2\left(1+\frac{14d}{\lambda}\right)^2} \tag{3}$$

where A is the Hamaker constant, R is the radius of the particle, d is the distance between the sphere and the plane, λ is the characteristic wavelength of the retardation, n is the number concentration of ions in the bulk, k_B is Boltzmann's constant, T is the absolute temperature, σ is the collision diameter and $\gamma_i = \tanh(\frac{e\psi_i}{4k_BT})$, where ψ_i is the surface potential, e is the charge of an electron, i indicates either the sphere or the plane, C_1, C_2, D_1, and D_2 are empirical coefficients and κ^{-1} is the Debye length. The Debye length may be computed as $\kappa^{-1} = 0.304/\sqrt{I}$ in monovalent salt solutions and $\kappa^{-1} = 0.176/\sqrt{I}$ in divalent salt solutions, where I is the ionic strength of the solution [23].

Ohshima's theory models the surface potential of a particle comprised of a hard core coated with a charged polymer layer with the following equation [36]:

$$\psi(d) = \psi_{donnan} + (\psi_0 + \psi_{donnan})e^{k_m x} + \frac{2k_BT}{ve} \times \ln\left[\frac{1+\tanh\left(\frac{ve\varsigma}{4k_BT}\right)e^{-k_m(x+L_0)}}{1-\tanh\left(\frac{ve\varsigma}{4k_BT}\right)e^{-k_m(x+L_0)}}\right] \tag{4}$$

where ψ_{donnan} is the Donnan potential, d is the particle separation distance, L_0 is the thickness of the polymer layer, ς is the zeta potential of the bare core of the composite particle, and $-L_0 \leqslant x \leqslant 0$ is a local coordinate which spans the thickness of the polymer layer at the hard particle surface.

The original formulation of Ohshima's theory does not account for hydration and steric forces, which are expected to be of importance in this study. Hydration forces should be taken into consideration whenever the hydrophilic nature of the interacting surfaces causes them to be hydrated. Iron oxides [42–47], silica [48,49], and borosilicate [50,51] are reported to be hydrophilic. The pumice stone employed in our study is also likely hydrated as it is mainly quartz, which is hydrophilic [52,53]. The sodium salt of CMC is also soluble in water and hydrophilic. Hydration forces are repulsive

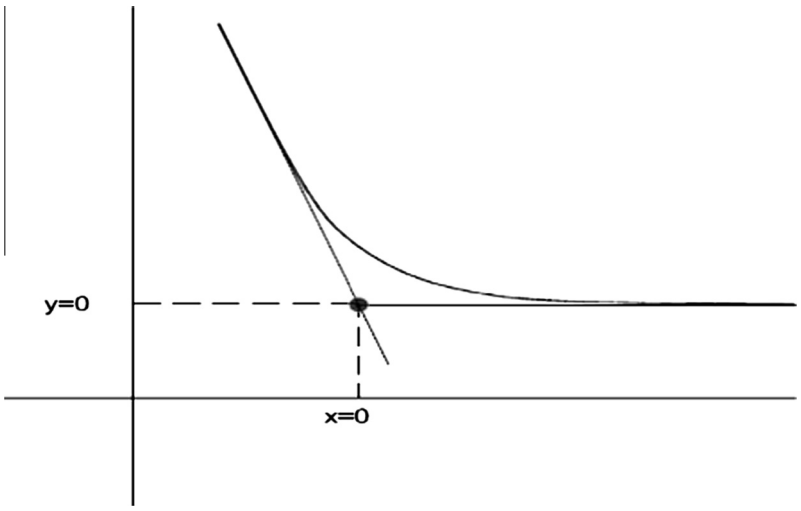

Fig. 2a. Schematics of how the repulsive approach curves are registered when no jump to contact is observed

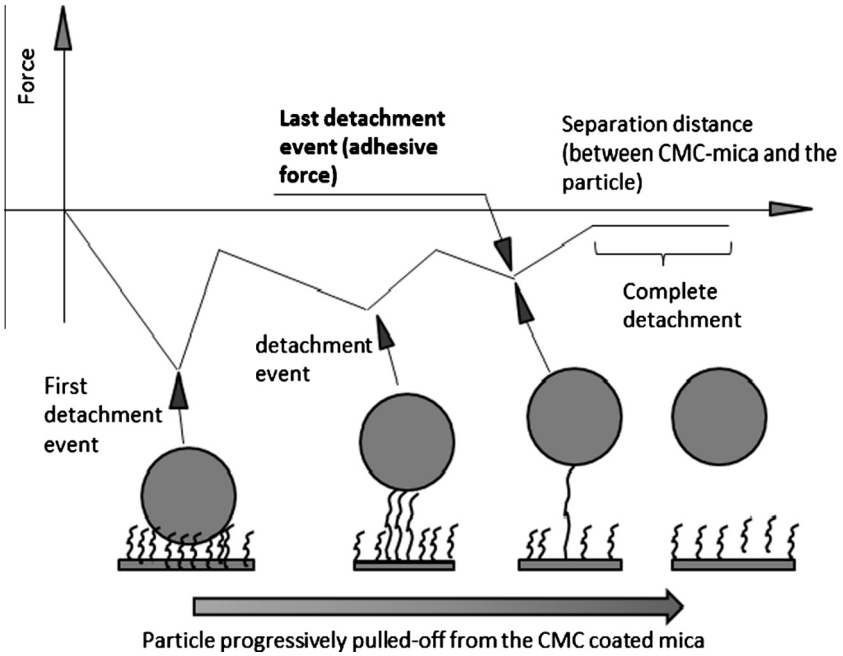

Fig. 2b. Schematics of different rupture events during mineral particle pull-off from the CMC coated substrate.

and arise due to changes in the water structure at the solid–liquid interface [48], polarization of water molecules [54], adsorption of ions at the solid–liquid interface, variations in the dielectric constant of the liquid, and formation of hydrogen bonds between the water molecules and the surface [55]. Steric forces result from the osmotic pressure arising when polymer chains are compressed upon approach to another surface. In the case of two surfaces coated by a polymer layer of thickness v, steric forces are described by the following expression [56]:

$$F_{steric} \approx k_B T \Gamma^{3/2} \left[\left(\frac{2L_0}{d} \right)^{9/4} - \left(\frac{d}{2L_0} \right)^{3/4} \right] \quad (5)$$

where Γ is the grafting density of the polymers. This expression is valid only for $\frac{L_0}{d} < 1$, as steric forces are zero when the polymer strands are not compressed, i.e., when $d \geqslant L_0$. Since, in our study, only the substrates were polymer coated while the particles employed were not, Eq. (2) was modified by substituting L_0 for $2L_0$. The optimal parameters for the modified Ohshima's model were found by minimizing the sum of the squared differences between the estimated and the predicted values using the Solver tool in Microsoft Excel.

2.2. QCM-D studies

2.2.1. Quartz-crystal microbalance with dissipation monitoring (QCM-D) system

Adsorption of the CMC polymer onto synthetic aluminum–silicate and silica substrates was studied with a QCM-D system (Q-Sense, Biolin Scientific, Sweden). This system is equipped with a flow cell, the bottom of which comprised a quartz sensor coated with the material of interest. The sensor is intermittently oscillated by two electrodes at different frequencies, corresponding to the

resonant frequency and overtones. Changes in the resonant frequency and overtones reflect film formation on the sensor surface, while changes in the dissipation parameter are related to the stiffness of the deposited films. These parameters are coupled to the overtones and the resonant frequency and are given by the following expression:

$$D_i(t) = \frac{1}{\pi \cdot f_{diff,i} \tau_i} \quad (6)$$

where t is the time, i denotes the overtone considered, $D_i(t)$ is the dissipation parameter for each overtone, $f_{diff,i} = f_i - f_{o,i}$, f_i is the current frequency of the overtone, τ_i is the time decay constant, and $f_{o,i}$ is the frequency of the overtone measured during calibration [32,57–60].

2.2.2. Mineral substrates used for QCM-D

Substrates sputter-coated with aluminum–silicates (QSX 999), silica (QSX 303), and magnetite (QSX 326) were purchased from Q-Sense. The atomic percent of the elements constituting the aluminum–silicate (AlSi) surface and magnetite were the following: AlSi: Si: 22.6%, Al: 11.4%, O: 65.2%, Ar: 0.8%; magnetite: Fe: 41.6%, O: 58.4%. As they were not in powder form, we could not determine the point of zero charge (PZC) for the materials coating the sensors.

Some authors have reported that magnetite's PZC may range between 6 and 7 [61,62], yet this value may be in question [63,64]. The PZC for aluminum–silicates depends on how the atoms are coordinated as well as composition. In particular, the higher the silicon content, the lower the PZC. In general, the PZC for aluminum–silicates is reported to be at acidic pH values (pH = 4 [65] or lower [66–68]) with the PZC for silica is reported to be at ~pH 2 [49,69–72].

2.2.3. Aqueous solutions

The chemistry of the polymer-free reference solutions is given in Table 2. Buffering to a pH of 4 or 8 was obtained by using $NaHCO_3$ or acetate, respectively. Solutions containing polymer were obtained by adding polymer to the originally polymer-free solutions, at a concentration of 0.25 g/L. CMC (MW: 90,000 g/mol, degree of substitution 0.7) was obtained from Sigma–Aldrich (product # 419273).

2.2.4. QCM-D methodology

The QCM-D experiments involved the five following steps. First, a stable baseline was acquired in Milli-Q water. Second, a polymer-free reference solution was injected in the flow cell. Third, a CMC containing solution was injected in the flow cell. Fourth, the flow cell was flushed with a polymer-free reference solution. Rinse-off with Milli-Q water followed.

3. Results and discussion

3.1. Forces of interaction between CMC and particles

Examples of AFM force curves acquired in the different water chemistries can be found in Figs. 3 and 4. AFM results for Milli-Q water at pH of 4, 5.5, and 8 revealed the presence of repulsive forces upon approach for all mineral particles and CMC except for CMC and iron oxide in Milli-Q water buffered to a pH of 4.0 (Table 3). Decreasing the Milli-Q pH from 5.5 to 4 decreased the average repulsion upon approach with silica, borosilicate, and pumice (Table 3). In the presence of divalent cations (100 mM $CaCl_2$, pH 5.5), attractive interactions were observed between all mineral types and CMC (Table 3). In the presence of monovalent cations (100 mM NaCl at pH 5.5), there was no evidence of any attractive interactions upon approach, indicating that CMC association is valence-dependent (Table 3). These data reveal that the forces upon approach were more significantly affected by the water chemistry and the mineral composition of the particles than by their surface roughness.

Adhesive forces were detected for all mineral particles in Milli-Q water at pH 4 and 5.5 and in 100 mM $CaCl_2$ at pH 5.5. In 100 mM NaCl, adhesive forces were significant for all particles except silica. When the pH of Milli-Q water was increased to 8 with addition of $NaHCO_3$, adhesive forces was negligible for all particles except borosilicate. Similar to the forces upon approach, adhesive forces were more significantly affected by the water chemistry and by the mineral composition of the particles than by their surface roughness.

In light of the reported PZC values for the various minerals, we examined the effect of solution chemistry on net forces of interaction as this allows for a direct interpretation of the relative influences of electrostatic, steric, and hydration forces on CMC-mineral surface association. The relative importance of these forces was analyzed using an extended Ohshima's theory (cf. Section 4) and shown in Figs. 5 and in Supporting Information (Figs. S1–S3). The analysis conducted demonstrated that van der Waals and steric forces played the most important role in the interactions

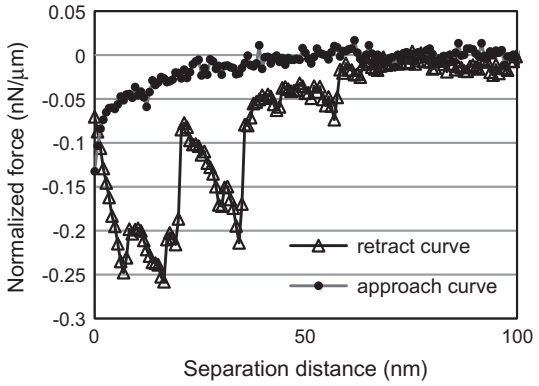

Fig. 3. Normalized AFM approach and retract force curves between CMC and iron oxide particles in 100 mM $CaCl_2$ solution.

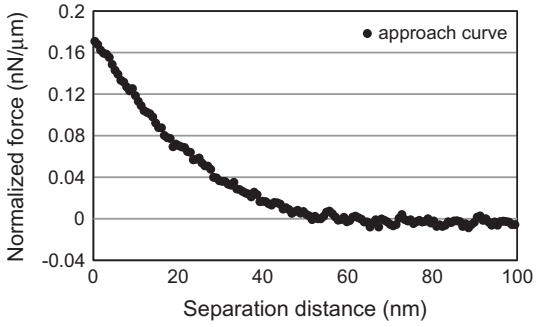

Fig. 4. Normalized AFM approach force curve in milli-Q buffered with $NaHCO_3$ (pH = 8) between CMC and iron oxide particles. Approach and retract curve coincided.

Table 2
Chemistry of the polymer-free reference solutions employed in QCM-D experiments.

Solution	Concentration	pH
NaCl	1, 10 and 100	4, 5.5 and 8
$CaCl_2$	1, 10 and 100	4, 5.5 and 8
milli-Q	N.A.	4, 5.5 and 8

Table 3
95% Confidence intervals for the normalized forces of interaction between CMC and mineral particles.

Solution	pH	Particle	Adhesive force (nN/μm)	Approach force, $x = 0$ ([b]) (nN/μm)
milli-Q	5.5	Iron oxide	−0.14 ± 0.09 ([a])	0.21 ± 0.06
		Silica	−0.07 ± 0.04 ([a])	0.22 ± 0.05
		Borosilicate	−0.03 ± 0.01 ([a])	0.17 ± 0.05
		Pumice	−0.13 ± 0.09 ([a])	0.20 ± 0.13
Milli-Q buffered with acetate	4	Iron oxide	−0.28 ± 0.17	−0.04 ± 0.02
		Silica	−0.05 ± 0.03 ([a])	0.10 ± 0.06
		Borosilicate	−0.05 ± 0.02	0.08 ± 0.04
		Pumice	−0.23 ± 0.1 ([a])	0.06 ± 0.09
Milli-Q buffered with $NaHCO_3$	8	Iron oxide	Negligible	0.29 ± 0.06
		Silica	Negligible	0.12 ± 0.02
		Borosilicate	−0.04 ± 0.01 ([a])	0.15 ± 0.03
		Pumice	Negligible	0.25 ± 0.08
100 mM NaCl	5.5	Iron Oxide	−0.18 ± 0.06 ([a])	0.00 ± 0.02
		Silica	Negligible	0.02 ± 0.01
		Borosilicate	−0.07 ± 0.03 ([a])	0.08 ± 0.03
		Pumice	−0.13 ± 0.05 ([a])	0.08 ± 0.04
100 mM $CaCl_2$	5.5	Iron oxide	−0.26 ± 0.16	−0.13 ± 0.04
		Silica	−0.15 ± 0.06	−0.02 ± 0.01
		Borosilicate	−0.07 ± 0.02 ([a])	−0.04 ± 0.05
		Pumice	−0.12 ± 0.04	−0.03 ± 0.01

[a] Negligible in some cases.
[b] Force measured at the point of contact between the particles and the substrate, negative values represent attraction, and positive values represent repulsion.

between particles and substrates, and that hydration forces were also significant. In Milli-Q water at pH 5.5 and 8, upon approach, repulsive forces dominate over attractive interactions between CMC and all minerals used. Reducing pH to 4 would reduce steric repulsion due to changes in CMC conformation. Electrostatic repulsion between CMC and silica, borosilicate and pumice should also be weakest at pH 4, as at pH 4, the negative charge density of CMC and the mineral particles would be lower than at pH 5.5 and 8. Electrostatic forces with iron oxide particles would be most attractive at pH 4, weakening at pH 5.5 and negligible at pH 8, which is close to the PZC of iron particles. These pH effects also explain the negligible adhesive forces seen for all particles with the exception of borosilicate in Milli-Q buffered to pH 8.

The data illustrate the effect of cation concentration and valence on damping repulsion upon approach between the CMC and the mineral surfaces. Ion binding to CMC can weaken electrostatic repulsion between CMC chains and favor their coiled conformation [26], thus reducing steric repulsion with all mineral particles. Na^+ [9] and Ca^{2+} [27,28] can both bind CMC chains, but Ca^{2+} should be more effective in screening CMC charge compared to Na^+, due to its higher valence. Ca^{2+} is therefore expected to promote more significantly coiled conformation for CMC than Na^+, as the interchain repulsion between CMC chains is weakest when their charge is close to neutral. Cations should also reduce electrostatic repulsion between CMC and silica, borosilicate and pumice.

Salts appeared to have minor effects on the adhesive forces for all but silica in 100 mM NaCl at pH 5.5, in which adhesion with CMC was negligible. Although NaCl reduces repulsion upon approach, the minor effects can be attributed to reduced hydrogen bonding between CMC and silica in the presence of Na^+ ions. Silanols at the silica surface are responsible for the formation of hydrogen bonds in pure water, but when Na^+ ions are present they may bind to the silanols [73], thus reducing their ability to sorb CMC through hydrogen bonding after contact occurs. It is noted that the hydrogen bonding length is approximately 2 Å and therefore shorter than the distance up to which electrostatic interactions can take place. This explains why NaCl reduces repulsion upon approach relative to pure water, yet damps adhesive forces (forces at contact) to negligible values. Ca^{2+} cations bound to silica are also deemed to reduce hydrogen bonding with CMC. However, Ca^{2+} is expected to be more effective than Na^+ in damping other repulsive interactions contributing to the overall measured adhesive force. The repulsive interactions include steric, hydration, and electrostatic forces. Calcium ions bound at the silica surface should also promote acid–base interactions with CMC, in agreement with the observations reported for starch [4]. The differences in composition between silica and the other mineral particles can account for the dissimilar impact of Na^+ ions on the individual forces at contact with CMC.

3.2. QCM-D study of cmc sorption onto mineral surfaces

3.2.1. Iron oxide (magnetite)

The adsorption of CMC onto various mineral surfaces was examined by QCM-D. In QCM-D experiments, the cell was flushed with polymer-free solution before and after the injection of the polymer solution. During injection of the polymer solution, CMC could sorb onto the mineral substrates. After being adsorbed, CMC molecules were subject to a shear force, due to the drag of the solution flowing in the laminar flow cell. In AFM experiments, the mineral particles were brought in contact with the CMC-coated mica and then pulled-off by applying a vertical pull-off force. Previous research showed that vertical pull-off forces and shear force can differ in magnitude [74,75], and QCM-D experiments thus provide information that complements AFM force spectroscopy data.

The differences in the third overtone and its dissipation before and after CMC injection are shown in Table 4. The differences refer to the parameter values measured: (a) in milli-Q water at the beginning of the experiment (baseline) and in milli-Q water after injection of CMC solution (rinse-off) and (b) in electrolyte solution before and after injection of CMC. For brevity, the differences are given only for the third overtone and its dissipation, but the other overtones followed similar trends. The CMC mass adsorbed onto the magnetite sensor surface is reported in Table 4. The adsorbed mass (ΔM) was estimated using the Sauerbrey equation [76]:

$$\Delta M = -C\frac{\Delta f_n}{n} \tag{7}$$

where n is the number of the overtone, Δf_n is the shift in the nth overtone, and C is 17.7 ng Hz^{-1} cm^{-2} for 5 MHz AT cut crystals.

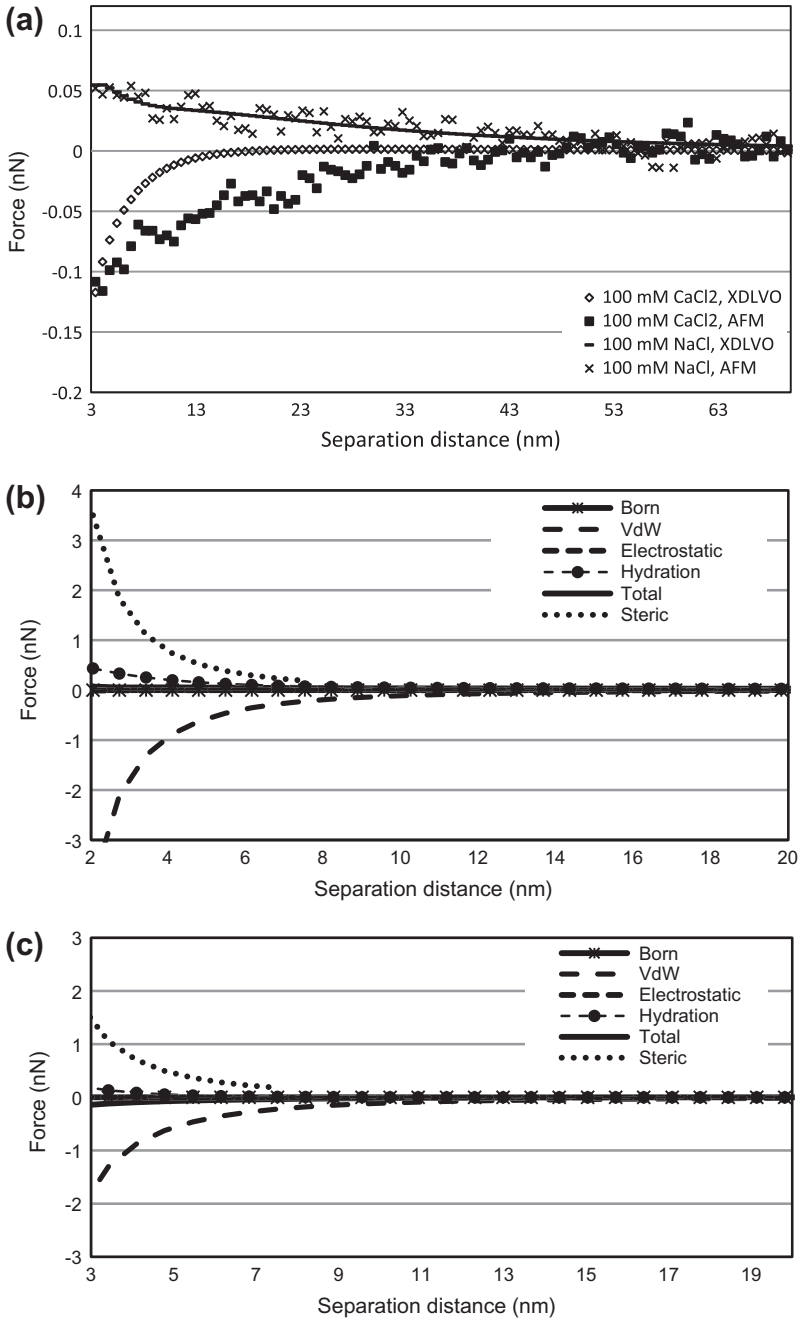

Fig. 5. (a) Comparison between predicted and experimental AFM forces between CMC coated mica and iron oxide particles in 100 mM NaCl and $CaCl_2$ (pH 5.5, *T* 23 °C); individual contributions of the forces in: (b) 100 mM NaCl (pH 5.5, *T* 23 °C); (c) 100 mM $CaCl_2$ (pH 5.5, *T* 23 °C).

This is a simplified equation that can slightly underestimate the adsorbed mass, but has been successfully used to model the sorption of large molecules such as lipids in QCM-D experiments [77].

The data reported in Table 4 revealed that after injection of CMC, the overtones were reduced to lower values, indicating polymer deposition at the sensor surface. Changes in the overtones can be related to mass deposition, with greater changes indicating greater mass adsorption. In many experiments, the dissipation factor increased after CMC injection. In particular, an increase in the dissipation factor was observed during those in which CMC deposition was most significant, i.e., when the decrease in the overtones was greatest. The dissipation factor is related to the decay of the waves propagating through films deposited at the sensor surface; specifically, the decay of the dissipation factor is most significant when films deposited at the sensor surface are thick and soft. The increase in the dissipation factor after CMC injection is therefore attributed to the softness of the polymeric films, as previously described for QCM-D experiments conducted using polymers [78,79].

Changes in the overtone data revealed that CMC adsorption is a pH- and ionic strength-dependent phenomenon (Table 4). Adsorption is favored at low pH and/or in the presence of high cation concentrations (or valency), as in these conditions, the changes in the overtones and in the dissipation factors are more significant than at high pH and low ionic strength. Our data also show that a greater CMC mass was *irreversibly* bound at the surface when CMC was allowed to adsorb onto iron oxide at low pH or high ionic strengths, as the changes in the overtones and the dissipation factors were

Table 4
Absolute value of the difference in the third overtone (F3) and its dissipation (D3) and Sauerbrey mass adsorbed during QCM-D experiments conducted with a magnetite sensor in different water chemistries.

Solution used during the CMC sorption step ([a])	pH	Ionic strength of salt solution (mM)	Absolute value of the difference between the parameters in salt solution before and after CMC injection			Absolute value of the difference between the parameter in milli-Q before and after CMC injection		
			F3 (Hz)	Mass (ng/cm^2)	D3 (−)	F3 (Hz)	Mass (ng/cm^2)	D3 (−)
Milli-Q	5.5	–	–		–	1	5.9	~0
1 mM NaCl		1	2.5	14.75	~0	2.5	14.75	~0
10 mM NaCl		10	4.4	25.96	~0	4.3	25.37	~0
100 mM NaCl		100	12.3	72.57	1.0	5.5	32.45	~0
1 mM $CaCl_2$		3	7.6	44.84	~0	5.4	31.86	~0
10 mM $CaCl_2$		30	24.2	142.78	1.3	13.8	81.42	2.1
100 mM $CaCl_2$		300	38.2	225.38	3.2	37.6	221.84	7.3
Milli-Q	4	–	–		–	8.3	48.97	~0
Milli-Q, pH 8	8	–	–		–	~0	0	~0
1 mM NaCl, pH 8		1	~0	0	~0	~0	0	~0
100 mM NaCl, pH 8		100	9.0	53.1	1.6	2.9	17.11	~0
1 mM $CaCl_2$, pH 8		3	7.6	44.84	2.4	3.0	17.7	~0
100 mM $CaCl_2$, pH 8		300	47.2	278.48	4.9	45.0	265.5	11.7

[a] The CMC polymer concentration in the sorption step was 0.25 g/l in all experiments.

significant even after rinse-off with Milli-Q water (Table 4). In light of these findings, it is proposed that when sorption of CMC to iron oxide occurs at low pH, or in the presence of salts, strong bonds are formed between the deposited CMC molecules and iron oxide as well as between various layers of CMC, and that these bonds remain stable even when the ionic strength was lowered or the pH raised, preventing detachment of CMC molecules from the substrate. The characteristics (e.g., valence) of the cation that was present in solution when CMC deposition occurred was also critical. Specifically, the data indicate that adsorption is greater in the presence of Ca^{2+} than of Na^+, even when $CaCl_2$ solutions have lower ionic strength than NaCl solutions. This may be a consequence of a reduction in CMC chain solubility upon sorption of Ca^{2+} ions. Moreover, Ca^{2+} could bind CMC molecules and reduce their negative charge density, damping electrostatic repulsion between CMC molecules. Therefore, in the presence of Ca^{2+}, deposition of CMC from solution onto pre-existing CMC layers on iron oxide occurred due to both reduced electrostatic repulsion between CMC molecules and inter-CMC hydrophobic interactions. The importance of Ca^{2+} in promoting acid–base interactions also cannot be discounted.

At pH 8, attachment appeared unfavorable in Milli-Q water, but CMC sorption at this same pH was observed in the presence of $CaCl_2$ (1 mM or higher) or in the presence of 100 mM NaCl. In addition to favoring cross-linking between CMC molecules, cations are expected to bind at the iron oxide (magnetite) surface, which should be close to its PZC at pH 8, thus increasing the number of positively charged sites onto which negatively charged CMC could attach. Calcium ion sorption on iron oxide was previously observed in $NaHCO_3$ solutions buffered to pH 8.5 [80] and sodium sorption should also occur. It is reasonable to speculate that CMC adsorption onto sites on the iron oxide surface should be greater in the presence of divalent cations. This hypothesis is supported by previous studies, which showed that divalent salts were more effective than monovalent salts in promoting CMC sorption onto negatively charged substrates [11].

It is noted that CMC sorption onto iron oxide was indicated by QCM-D measurements even in milli-Q at pH 5.5 and 100 mM NaCl solutions at pH 5.5, in which AFM experiments indicated the presence of adhesive forces, but showed repulsive and negligible forces prior to contact, respectively. Repulsive steric forces are expected to be more significant when iron oxide particles approach a thick polymer brush physisorbed onto mica compared to when CMC molecules dispersed in solution approach an iron oxide surface. However, QCM-D and AFM experiments provided similar trends regarding the role of water chemistry on attachment onto iron oxides, indicating that high ionic strengths and specifically $CaCl_2$ salt promote CMC attachment, while high pH values hinder it in the absence of $CaCl_2$ or NaCl salts.

3.2.2. Silica and aluminum–silicate

QCM-D experiments were conducted with Milli-Q water as well as 100 mM NaCl and $CaCl_2$ solutions. A summary of these experiments is given in Table 5. In all water chemistries (including 100 mM $CaCl_2$ solutions), the overtones and dissipation values returned to their baseline values once the flow cell was flushed with either salt solutions or milli-Q, indicating that attachment was weak and reversible. These results are consistent with AFM measurements, which revealed weak adhesive forces in all chemistries and repulsion upon approach in all chemistries but 100 mM $CaCl_2$ (see Table 3).

4. Application of the modified Ohshima's model

Modeling was conducted for curves acquired in 100 mM NaCl and 100 mM $CaCl_2$ solutions at pH 5.5, in order to understand the roles of the interaction forces and investigate which were the most important components of the interactions between mineral particles and CMC-coated substrates. Comparisons between the predicted and the experimental curves and the contributions of each force are given in Fig. 5 and in Supporting Information (Figs. S1–S3). These data reveal that the Ohshima model provides a good fit to the experimental data for separation distances of 2–5 nm. The optimal values of the parameters are given in Supporting Information (Tables S1–S8). The modeling data highlight that steric and van der Waals forces played a major role in the interactions between mineral particles and CMC-coated substrates, and that hydration forces were also important. The magnitude of the steric and the hydration forces demonstrate the value of using a modified

Table 5
Synoptic overview of QCM-D experiments conducted using silica and aluminum–silicate sensors.

pH	Solution used during the CMC sorption step ([a])
5.5	Milli-Q 100 mM NaCl 100 mM $CaCl_2$
4	Milli-W
8	Milli-Q

[a] The CMC polymer concentration in the sorption step was 0.25 g/l in all experiments.

version of Ohshima's model that accounts for these effects. However, it was noted that while hydration forces depend solely on the water chemistry and on the surface properties of the interacting surfaces, the magnitude of the steric forces is dependent on the thickness of the polymer layer. Therefore, while in our AFM experiments steric forces were significant due to the thick CMC layer with which mica disks were coated, they are expected to play a less significant role in the presence of thin polymer coatings. In particular, we believe that steric forces were less significant in QCM-D tests than in AFM experiments, as discussed in Section 3.2.1.

5. Conclusions

Forces of interaction between a sodium salt of CMC and different minerals were studied using AFM and QCM-D at different ionic strengths and pH values. CMC attachment to silicates and aluminum–silicates was unfavorable in all chemistries except 100 mM $CaCl_2$ at pH 5.5, in which it was nonetheless weak and reversible. Sorption of CMC onto silicates was least favorable in Milli-Q water buffered to pH 8, in which the forces upon approach were repulsive and adhesive forces were negligible for all but borosilicate. These findings indicate that it is desirable to operate at slightly acidic pH values and in the presence of salts if CMC is employed to stabilize silicate particle suspensions, as such conditions would promote CMC sorption onto silicates.

CMC attachment onto iron oxides was irreversible in all chemistries except at pH 8 in low ionic strength solutions (Milli-Q and 1 mM NaCl) and was most significant at high ionic strength and low pH values. These data demonstrate that CMC has the potential of stabilizing suspensions of iron oxide coated particles employed for remediation purposes, as it is able to sorb onto iron particles and should contribute steric repulsion with neighboring particles.

It is noted that in our study, we only investigated the ability of CMC to sorb onto mineral particles, but we have not probed the forces between CMC-coated mineral particles. In order to stabilize particles, CMC must (1) sorb onto the particles providing good coverage and (2) contribute significant repulsive forces to the interaction between CMC-coated particles, preventing their aggregation. Further studies probing the forces of interaction between CMC-coated particles would be useful to elucidate if the latter condition is fulfilled.

Our study has further shown that, due to the repulsive forces between CMC and silicates in all chemistries but 100 mM $CaCl_2$ at pH 5.5, iron particles stabilized with CMC polymer should be mobile in soils that are primarily silicate minerals in many water chemistries. Conversely, if the soils contain iron oxide minerals, attachment of CMC-coated iron particles to the iron oxide minerals is expected to hinder transport.

A modified version of Ohshima's theory was suitable to represent our experimental AFM data. Modeling highlighted that in AFM experiments, the interactions between mineral particles and CMC were dominated by van der Waals and steric forces, and that hydration forces were also important.

Acknowledgments

This work was funded by the Natural Sciences and Research Council of Canada through a Strategic Projects Grant.

Appendix A. Supplementary material

Supplementary data associated with this article can be found, in the online version, at http://dx.doi.org/10.1016/j.jcis.2013.03.053.

References

[1] C.W. Hoogendam, A. De Keizer, M.A. Cohen Stuart, B.H. Bijsterbosch, J.G. Batelaan, P.M. Van der Horst, Langmuir 14 (1998) 3825.
[2] S. Bayarri, L. Gonzalez-Tomas, E. Costell, Food Hydrocolloids 23 (2009) 441.
[3] J. Wang, P. Somasundaran, J. Colloid Interface Sci. 291 (2005) 75.
[4] Q. Liu, Y. Zhang, J.S. Laskowski, Int. J. Miner. Process. 60 (2000) 229.
[5] K.C. Corin, P.J. Harris, Miner. Eng. 23 (2010) 915.
[6] R.J. Pugh, Int. J. Miner. Process. 25 (1989) 101.
[7] E. Grzadka, Cellulose 18 (2011) 291.
[8] O. Bicak, Z. Ekmekci, D.J. Bradshaw, P.J. Harris, Miner. Eng. 20 (2007) 996.
[9] A. Mierczynska-Vasilev, D.A. Beattie, Miner. Eng. 23 (2010) 985.
[10] A. Beaussart, A. Mierczynska-Vasilev, D.A. Beattie, J. Colloid Interface Sci. 346 (2010) 303.
[11] M. Khraisheh, C. Holland, C. Creany, P. Harris, L. Parolis, Int. J. Miner. Process. 75 (2005) 197.
[12] E. Burdukova, C.G. Van Leerdam, F.E. Prins, R.G. Smeink, D.J. Bradshaw, J.S. Laskowski, Miner. Eng. 21 (2008) 1020.
[13] L.T. Cuba-Chiem, L. Huynh, J. Ralston, D.A. Beattie, Miner. Eng. 21 (2008) 1013.
[14] L.A.S. Parolis, R. van der Merwe, G.C. van Leerdam, F.E. Prins, R.G. Smeink, Miner. Eng. 20 (2007) 970.
[15] F. He, D. Zhao, J. Liu, C.B. Roberts, Ind. Eng. Chem. Res. 46 (2007) 29.
[16] F. He, D. Zhao, Environ. Sci. Technol. 41 (2007) 6216.
[17] J. Fatisson, S. Ghoshal, N. Tufenkji, Langmuir 26 (2010) 12832.
[18] N. Sakulchaicharoen, D.M. O'Carroll, J.E. Herrera, J. Contam. Hydrol. 119 (2011) 1.
[19] S.H. Joo, S.R. Al Abed, T. Luxton, Environ. Sci. Technol. 43 (2009) 4954.
[20] R.N. Lerner, Q. Lu, H. Zeng, Y. Liu, Water Res. 46 (2012) 975.
[21] T. Long, C.A. Ramsburg, J. Hazard. Mat. 189 (2011) 801.
[22] E. Pensini, B.E. Sleep, C.M. Yip, D.M. O'Carroll, Environ. Sci. Technol. (2012).
[23] J. Israelachvili. Intermolecular and surface forces, Academic Press, San Diego, 1992.
[24] M. Stamm Polymer. surfaces and interfaces, Springer-Verlag, Berlin, 2008
[25] R. Wach, H. Mitomo, N. Nagasawa, F. Yoshii, Radiat. Phys. Chem. 68 (2003) 771.
[26] U. Kästner, H. Hoffmann, R. Dönges, J. Hilbig, Coll. Surf. A 307 (1997) 307.
[27] A.J. Varma, V.B. Chavan, Carbohydr. Polym. 45 (2001) 101.
[28] L. Järnström, P. Stenius, Coll. Surf. A 50 (1990) 47.
[29] R.D. Hill, J.G. Zadow, J. Dairy Res. 45 (1978) 77.
[30] N.S. Schneider, P. Doty, J. Phys. Chem. 58 (1954) 762.
[31] B. Porsch, B. Wittgren, Carbohydr. Polym. 59 (2005) 27.
[32] H. Orelma, I. Filpponen, L.-S. Johansson, J. Laine, O.J. Rojas, Biomacromolecules 12 (2011) 4311.
[33] Z. Liu, H. Choi, P. Gatenholm, A.R. Esker, Langmuir 27 (2011) 8718.
[34] H. Li, M. Rief, F. Oesterhelt, H.E. Gaub, X. Zhang, J. Shen, Chem. Phys. Lett. 305 (1999) 197.
[35] H. Ohshima, Colloid Polym. Sci. 285 (2007) 1411.
[36] H. Ohshima, M. Nakamura, T. Kondo, Colloid Polym. Sci. 270 (1992) 873.
[37] I.L. Molnar, D.M. O'Carroll, J.I. Gerhard, J. Contam. Hydrol. 119 (2011) 1.
[38] M. Kosmulski, E. Maczka, E. Jartych, J.B. Rosenholm, Adv. Colloid Interface Sci. 103 (2003) 57.
[39] G.C.C. Yang, H.-C. Tu, C.-H. Hung, Sep. Purif. Technol. 58 (2007) 166.
[40] J.P. Cleveland, S. Manne, D. Bocek, P.K. Hansma, Rev. Sci. Instrum. 64 (1993) 403.
[41] B. Cappella, G. Dietler, Surf. Sci. Rep. 34 (1999) 5.
[42] J.G. Catalano, Geochim. Cosmochim. Acta 75 (2011) 2242.
[43] N.H. De Leeuw, T.G. Cooper, Geochim. Cosmochim. Acta 71 (2007) 1655.
[44] Y. Joseph, W. Ranke, W. Weiss, J. Phys. Chem. B 104 (2000) 3224.
[45] J. Majzlan, L. Mazeina, A. Navrotsky, Geochim. Cosmochim. Acta 71 (2007) 615.
[46] E. Tombácz, A. Hajdu, E. Illes, K. László, G. Garberoglio, P. Jedlovszky, Langmuir 25 (2009) 13007.
[47] T.P. Trainor, A.M. Chaka, P.J. Eng, M. Newville, G.A. Waychunas, J.G. Catalano, G.E.J. Brown, Surf. Sci. 573 (2004) 204.
[48] A. Grabbe, R.G. Horn, J. Colloid Interface Sci. 157 (1993) 375.
[49] P.G. Hartley, I. Larson, P.J. Scales, Langmuir 13 (1997) 2207.
[50] P.J. Van Zwol, G. Palasantzas, J.T.M. De Hosson, Phys. Rev. E 78 (2008).
[51] E. Bonaccurso, M. Kappl, H.-J. Butt, Phys. Rev. Lett. 88 (2002) 076103.
[52] V. Bolis, B. Fubini, L. Marchese, G. Martra, D. Costat, J. Chem. Soc. Faraday Trans. 87 (1991) 497.
[53] H. Nygren, M. Stenberg, J. Biomed. Mater. Res. 22 (1988) 1.
[54] J. Faraudo, F. Bresme, Phys. Rev. Lett. 94 (2005) 077802.
[55] J.J. Valle-Delgado, J.A. Molina-Bolívar, F. Galisteo-González, M.J. Gálvez-Ruiz, A. Feiler, M.W. Rutland, J. Chem. Phys. 123 (2005) 0347081.
[56] H.J. Butt, M. Kappl, H. Mueller, R. Raiteri, Langmuir 15 (1999) 2559.
[57] M. Rodahl, F. Höök, B. Kasemo, Anal. Chem. 68 (1996) 2219.
[58] M. Rodahl, F. Höök, A. Krozer, P. Brzezinski, B. Kasemo, Rev. Sci. Instrum. 66 (1995) 3924.
[59] C. Steinem, A. Janshoff. Piezoelectric sensors, Springer-Verlag, Berlin, 2007.
[60] M. Thompson, D. Stone. Surface-launched acoustic wave sensors: chemical sensing and thin-film characterization, John Wiley&Sons Inc., New York, 1997.
[61] P.H. Tewari, A.W. McLean, J. Colloid Interface Sci. 40 (1972) 267.
[62] M.A. Blesa, N.M. Figliolia, A.J.G. Maroto, A.E. Regazzoni, J. Colloid Interface Sci. 101 (1984) 410.
[63] A.P. Vieira, G. Berndt, I.G.J. de Souza, E. Di Mauro, A.J. Paesano, H. de Santana, A.C.S. da Costa, C.T.B.V. Zaia, D.A.M. Zaia, Amino Acids 40 (2011) 205.

[64] E. Illes, E. Tombácz, Colloids Surf. A 230 (2004) 99.
[65] A.A. Jara, S. Goldberg, M.L. Mora, J. Colloid Interface Sci. 292 (2005) 160.
[66] D.L. Gallup, Geothermics 26 (1997) 483.
[67] S. Gopalakrishnan, S. Yada, J. Muench, T. Selvam, W. Schwieger, M. Sommer, W. Peukert, Appl. Catal. A 327 (2007) 132.
[68] Y. Hu, X. Liu, Z. Xu, Miner. Eng. 16 (2003) 219.
[69] L.H. Allen, E. Niatijevic, J. Colloid Interface Sci. 31 (1969) 287.
[70] X. Cui, W.C. Zin, W.J. Cho, C.S. Ha, Mater. Lett. 59 (2005) 2257.
[71] V.K. Gupta, S. Sharma, Environ. Sci. Technol. 36 (2002) 3612.
[72] L.J. Meagher, J. Colloid Interface Sci. 152 (1992) 293.
[73] W.L.W. Hau, D.W. Trau, N.J. Sucher, M. Wong, Y. Zohar, J. Micromech. Microeng. 13 (2003) 272.
[74] Y. Ando, Wear 238 (2000) 12.
[75] L.-O. Heim, J. Blum, M. Preuss, H.-J. Butt, Phys. Rev. Lett. 83 (1999) 3328.
[76] J. Malmstrom, H. Agheli, P. Kingshott, D.S. Sutherland, Langmuir 23 (2007) 9760.
[77] R. Richter, A. Mukhopadhyay, A. Brisson, Biophys. J. 85 (2003) 3035.
[78] S.M. Notley, M. Eriksson, L. Wågberg, J. Colloid Interface Sci. 292 (2005) 29.
[79] J. Hedin, J.-E. Lofroth, M. Nyden, Langmuir 23 (2007) 6148.
[80] P. Roonasi, A. Holmgren, Surf. Interface Anal. 42 (2010) 1118.